Contribution to the *PEARL 2005 workshop, Physics at EBIT and Advanced Research Light Sources, 9-13th March, 2005, Sanya, Hainan, China*

Extreme ultraviolet spectroscopy of highly charged argon ions at the Berlin EBIT

C. Biedermann, R. Radtke, G. Fussmann, F.I. Allen

Institut für Physik der Humboldt-Universität zu Berlin, Lehrstuhl Plasmaphysik, Newtonstraße 15, 12489 Berlin and Max-Planck-Institut für Plasmaphysik, EURATOM Association

e-mail address: Christoph.Biedermann@physik.hu-berlin.de

Abstract. Extreme ultraviolet radiation from highly charged argon was investigated at the Berlin Electron Beam Ion Trap with a 2 m grazing incidence spectrometer. Lines in the wavelength range 150 to 660 Å originating from C-like Ar^{12+} to Li-like Ar^{15+} ions have been identified and are compared with database information from solar line lists and predictions. Line ratios for the observed resonance, intercombination and forbidden lines offer important diagnostic capabilities for low density, hot plasmas.

1. Introduction

The observation of radiation in the extreme-ultraviolet spectral range (EUV) from highly charged ions provides a versatile diagnostic tool for low density, hot plasmas, such as laser-produced laboratory plasmas, fusion plasmas or the plasma of astrophysical objects [1]. With the availability of data from missions like the Solar Ultraviolet Measurements of Emitted Radiation (SUMER) [2] there has been an increasing need for the comparison of astrophysical database information with experimental data obtained under well-controlled laboratory conditions. Information on the plasma state, the elemental abundance or temperature and density, can be inferred by measuring wavelengths and intensities of certain EUV spectral lines. However, conclusions about the intensity of observed spectral lines can only be drawn if a relationship between the measured line ratio and the excitation and emission of these lines exists under similar plasma conditions. This dependencies requires support by a theoretical model with *ab initio* calculations, which, on the other hand, requires verification by well-diagnosed experiments. An Electron Beam Ion Trap (EBIT) [3] provides a controlled laboratory plasma of highly charged ions being excited by an electron beam to emit radiation which is analysed by spectrometers. The conditions in an EBIT for the excitation of radiation resemble those of the upper solar atmosphere with similar electron densities ($n_e = 10^{12}$ cm^{-3}) and excitation primarily by electron collisions. EBIT can produce ions of any element of the periodic table in any charge state. Here, we want to focus on the investigation of the L-shell emission of argon ions. Argon is also abundant as a minor component of the solar atmosphere at temperatures of 0.2 to 1 keV emitting EUV spectral lines which are applied for diagnostics.

There is only scarce information on the L-shell emission of argon in line lists, e.g. NIST's Atomic Spectra Database has so far no entries for highly charged argon ions like C-like Ar^{12+} to Li-like Ar^{15+}. Some information is collected in the Kelly tables [4] from solar line lists [5-7] and theta-pinch experiments [8]. A proposal by Feldman [1] points out a few specific line ratios suitable for diagnostics with reference to wavelengths predictions by Edlén [9] and solar line lists [5-7]. Recently spectral information on Ar^{12+} became available by Liang et al. [10] applying the recently developed Flexible Atomic Code.

At the Berlin EBIT we have measured the EUV radiation of O-like Ar^{10+} to Li-like Ar^{15+} ions in the wavelength range 150 to 700 Å. In the contribution here, we present a comparison with the wavelengths available for Ar^{12+} to Ar^{15+} ions.

2. Experimental method

The Berlin EBIT uses a strongly compressed monoenergetic electron beam (6 to 90 mA) to produce highly charged ions by successive electron impact ionization. The ions are trapped radially by the space charge potential and excited by collisions with electrons [3]. Axial confinement is achieved by biasing (200 V) the end sections of the drift tube structure which also allows periodical (100 ms) emptying of the trap to prevent accumulation of high-Z background ions. The target specie argon is injected as neutral gas continuously into the trapping region.

The acceleration voltage of the electron beam is set in order to produce a particular highest charge state determined by the ionization potential of the ion species. Decreasing the acceleration voltage systematically limits the highest possible ionization stage and one observes now the radiation pattern of that ion to disappear as soon as its charge state can no longer be produced. The electron beam energy E_e is determined by the acceleration potential at the drift tube assembly, taking into account corrections for the space charge of the electron beam and the ion inventory of the trap. The uncertainty in E_e is ±20 eV originating from the estimate of the number of trapped ions and E_e has a spread of about 40 eV.

The EUV radiation emitted from the ions is analyzed with a high-resolution Schwob-Fraenkel grazing-incidence spectrometer [11]. A 6 m curvature grazing-incidence Au-plated mirror focuses the radiation from the 70 µm diameter, 16 mm high excitation region in the trap on the 18 µm wide entrance slit of the spectrometer, which is equipped with a 600 l/mm grating mounted at an angle of 2° with a blaze angle of 3.5°. The photons are detected by a MgF_2-coated micro-channel-plate stack followed by a phosphor screen image intensifier viewed by a thermoelectrically cooled charge-coupled device camera. The detector assembly moves with high precision along the Rowland circle, recording spectral information in the range 30 to 1000 Å. The wavelength scale was calibrated using the Lyman series of He^+ and well-known lines in first and second order diffraction from C- to Li-like Neon [4].

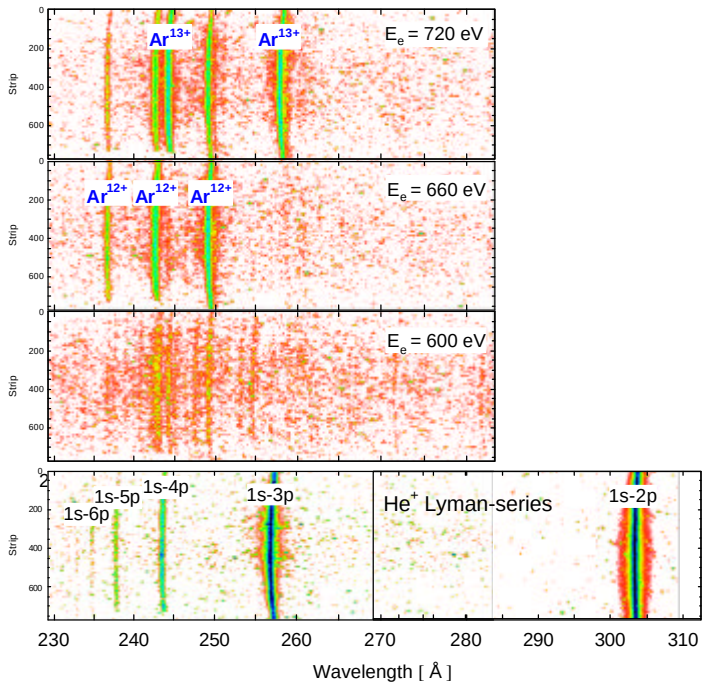

FIGURE 1. EUV-emission spectra of B-like Ar^{13+} and C-like Ar^{12+} ions at three different electron beam energies. The bottom plate shows the Lyman series of He^+ used to calibrate the wavelength axis.

3. Spectra

Figure 1 shows an example of CCD images demonstrating the technique to limit the emission of ions in EBIT to a selected charge state. While for an electron beam energy of 720 eV we can clearly see the 243 and 257 Å lines of Ar^{13+}, these lines vanish in the 660 eV spectrum below the ionization threshold for Ar^{12+} of 686 eV. In the third image E_e=600 eV is close to the ionization energy (618 eV) of Ar^{11+} and the Ar^{12+} EUV radiation ceases. The panel at the bottom shows the Lyman series of singly charged He-ions used for calibration of the wavelength scale, running EBIT with a very high gas injection pressure and short confinement times to increase emission from low-Z lowly charged ions.

TABLE 1. EUV lines of Li-, Be- and B-like argon ions. Comparison of experimental wavelengths in [Å] from the Berlin EBIT with data from solar spectra and predictions. The total uncertainty in the measured wavelength is marked as [x]. The observed strength of the line is rated as vs (very strong), s (strong), m (moderate), w (weak) and vw (very weak). The Kelly tables [4] refer to solar line lists and experiments. The numbers proposed by Feldman [1] are based on predictions by Edlén [9]. The ground state (gs) of Li-like Ar^{15+} $1s^2\ 2s\ ^2S_{1/2}$ has an ionization potential I.P. of 918.04 eV, of Be-like Ar^{14+} $1s^2\ 2s^2\ ^1S_0$, I.P. 854.78 eV and of B-like Ar^{13+} $1s^2\ 2s^2\ 2p\ ^2P_{1/2}$, I.P. 755.75 eV. 'bl' marks a blend with lines from second order reflection.

Ion	lower level	upper level	Berlin EBIT		wavelength	
			wavelength	strength	Kelly [4]	Feldman [1]
Ar^{15+}	$1s^2\ 2s\ ^2S_{1/2}$	$1s^2\ 2p\ ^2P_{3/2}$	353.921 [6]	vs	353.92[a]	
Ar^{15+}	$1s^2\ 2s\ ^2S_{1/2}$	$1s^2\ 2p\ ^2P_{1/2}$	389.108 [7]	s	389.14[a]	
Ar^{14+}	$1s^2\ 2s^2\ ^1S_0$	$1s^2\ 2s\ 2p\ ^1P_1$	221.157 [21]	vvs	221.15[b]	
Ar^{14+}	$1s^2\ 2s^2\ ^1S_0$	$1s^2\ 2s\ 2p\ ^3P_1$	424.022 [13]	w	424.01[b]	424.01[c]
Ar^{13+}	$2s^2\ 2p\ ^2P_{1/2}$	$2s\ 2p^2\ ^2P_{3/2}$	180.253 [63]	m	180.29[d]	180.292
Ar^{13+}	$2s^2\ 2p\ ^2P_{1/2}$	$2s\ 2p^2\ ^2P_{1/2}$	183.417 [54]	m	183.41[d]	183.450
Ar^{13+}	$2s^2\ 2p\ ^2P_{3/2}$	$2s\ 2p^2\ ^2P_{3/2}$	187.930 [52]	vs	187.95[d]	187.969
Ar^{13+}	$2s^2\ 2p\ ^2P_{3/2}$	$2s\ 2p^2\ ^2P_{1/2}$	191.363 [51]	s	191.35[d]	191.404
Ar^{13+}	$2s^2\ 2p\ ^2P_{1/2}$	$2s\ 2p^2\ ^2S_{1/2}$	194.354 [52]	vs	194.39[d]	194.396
Ar^{13+}	$2s^2\ 2p\ ^2P_{3/2}$	$2s\ 2p^2\ ^2S_{1/2}$	203.374 [63]	w	203.35[d]	203.351
Ar^{13+}	$2s\ 2p^2\ ^4P_{1/2}$	$2p^3\ ^4S_{3/2}$	204.28 [50]	vw	204.64[d]	204.668
Ar^{13+}	$2s\ 2p^2\ ^4P_{3/2}$	$2p^3\ ^4S_{3/2}$	208.98 [60]	vw	208.31[d]	208.329
Ar^{13+}	$2s\ 2p^2\ ^4P_{5/2}$	$2p^3\ ^4S_{3/2}$	213.22 [31]	vw	213.42[d]	213.439
Ar^{13+}	$2s^2\ 2p\ ^2P_{1/2}$	$2s\ 2p^2\ ^2D_{3/2}$	243.895 [95]	s	243.74[d]	243.829
Ar^{13+}	$2s^2\ 2p\ ^2P_{3/2}$	$2s\ 2p^2\ ^2D_{5/2}$	257.372 [39]	m	257.37[d]	257.446
Ar^{13+}	$2s^2\ 2p\ ^2P_{3/2}$	$2s\ 2p^2\ ^2D_{3/2}$	257.967 [45]	m	257.98[d]	258.084
Ar^{13+}	$2s\ 2p^2\ ^2P_{1/2}$	$2p^3\ ^2D_{3/2}$	376.732 [6]	vs		376.22
Ar^{13+}	$2s\ 2p^2\ ^2P_{3/2}$	$2p^3\ ^2D_{5/2}$	389.719 [10]	s		387.37
Ar^{13+}	$2s^2\ 2p\ ^2P_{1/2}$	$2s\ 2p^2\ ^4P_{3/2}$	420.465 [97]	vw		420.37
Ar^{13+}	$2s^2\ 2p\ ^2P_{1/2}$	$2s\ 2p^2\ ^4P_{1/2}$	436.698 [44]bl	w		436.11
Ar^{13+}	$2s^2\ 2p\ ^2P_{3/2}$	$2s\ 2p^2\ ^4P_{5/2}$	441.059 [76]	vw		441.07
Ar^{13+}	$2s^2\ 2p\ ^2P_{3/2}$	$2s\ 2p^2\ ^4P_{3/2}$	464.634 [95]	vw		464.61
Ar^{13+}	$2s^2\ 2p\ ^2P_{3/2}$	$2s\ 2p^2\ ^4P_{1/2}$	484.944 [90]	vw		483.92

[a] solar line list, Sandlin et al. [5]
[b] Ref. [7] and solar line list, Sandlin et al. [5]
[c] solar line list, Dere [6]
[d] theta-pinch plasma experiment [8]

For the evaluation of accurate line positions a horizontal, central 100 pixel wide strip was binned perpendicular to the dispersion direction to circumvent the slight curvature of the slit image on the CCD blurring the wavelength information. Peaks in the binned spectra are fitted with Gaussian functions and the results are summarized in Tables 1 and 2.

TABLE 2. EUV lines from C-like argon ions (Ar^{12+}), gs $1s^2\ 2s^2\ 2p^2\ ^3P_0$, I.P. 686.11 eV. Comparison of experimental wavelengths from the Berlin EBIT with predictions from the Kelly data tables [4], Feldman [1] and Liang [10].

lower level	upper level	Berlin EBIT		wavelength		
		wavelength	strength	Kelly [4]	Feldman [1]	Liang [10]
$2s^2\ 2p^2\ ^3P_0$	$2s\ 2p^3\ ^3S_1$	159.060 [70]	w	159.08[a]		159.089
$2s^2\ 2p^2\ ^3P_1$	$2s\ 2p^3\ ^3S_1$	161.611 [90]	w	161.61[a]		161.624
$2s^2\ 2p^2\ ^1D_2$	$2s\ 2p^3\ ^1P_1$	163.010 [78]	m	162.96[a]		162.980
$2s^2\ 2p^2\ ^3P_2$	$2s\ 2p^3\ ^3S_1$	164.826 [54]	s	164.82[a]		164.819
$2s^2\ 2p^2\ ^1D_2$	$2s\ 2p^3\ ^1D_2$	184.843 [77]	s	184.90[b]		184.433
$2s^2\ 2p^2\ ^1S_0$	$2s\ 2p^3\ ^1P_1$	186.333 [52]	w	186.38[b]		186.414
$2s^2\ 2p^2\ ^3P_0$	$2s\ 2p^3\ ^3P_1$	201.689 [58]	m	201.69[b]		201.711
$2s^2\ 2p^2\ ^3P_1$	$2s\ 2p^3\ ^3P_2$	205.257 [51]	w	205.24[b]		205.287
$2s^2\ 2p^2\ ^3P_1$	$2s\ 2p^3\ ^3P_1$	205.628 [21]	m	205.77[b]		205.804
$2s^2\ 2p^2\ ^3P_1$	$2s\ 2p^3\ ^3P_0$	205.839 [60]	s	205.94[b]		205.950
$2s^2\ 2p^2\ ^3P_2$	$2s\ 2p^3\ ^3P_2$	210.537 [68]	vs	210.46[b]		210.468
$2s^2\ 2p^2\ ^3P_2$	$2s\ 2p^3\ ^3P_1$	211.107 [113]	s	211.00[b]		
$2s^2\ 2p^2\ ^3P_0$	$2s\ 2p^3\ ^3D_1$	236.249 [21]	m	236.27[b]		236.285
$2s^2\ 2p^2\ ^3P_1$	$2s\ 2p^3\ ^3D_1$	241.898 [79]	vvw	241.90[b]		241.921
$2s^2\ 2p^2\ ^3P_1$	$2s\ 2p^3\ ^3D_2$	242.199 [10]	s	242.22[b]		242.240
$2s^2\ 2p^2\ ^3P_2$	$2s\ 2p^3\ ^3D_3$	248.626 [9]	s	248.68[b]		248.697
$2s^2\ 2p^2\ ^3P_2$	$2s\ 2p^3\ ^3D_2$	249.438 [35]	w	249.46[b]		249.487
$2s^2\ 2p^2\ ^3P_1$	$2s\ 2p^3\ ^5S_2$	463.413 [94]	vvw	462.8[c]	459.53[d]	459.530
$2s^2\ 2p^2\ ^3P_2$	$2s\ 2p^3\ ^5S_2$	486.359 [70]	m	490.2[c]	486.33[d]	486.328
$2s^2\ 2p^2\ ^3P_1$	$2s^2\ 2p^2\ ^1S_0$	659.562 [89]	w	657[e]	656.60[f]	656.604

[a] Deutschman et al. [12]

[b] theta-pinch plasma experiment [8]

[c] Kastner et al. [13]

[d] predicted by Edlén [14]

[e] Kelly tables [4] and theta-pinch plasma experiment [8]

[f] Feldman et al. [15]

4. Comparison with database information

The observed spectral lines are identified by cross-referencing to previous measurements and multi-channel Dirac-Fock calculations by Edlén. The two measured Ar^{15+} EUV lines connect the excited $1s^2 2p\ ^2P_{1/2}$ and $^2P_{3/2}$ levels with the ground state. These two levels can also be fed by the so-called *j* and *k* satellites of Li-like argon observed in the x-ray spectral region. The line ratio of these satellites populated by dielectronic recombination and the *w*-resonance line of He-like Ar^{16+} serves as a temperature diagnostic for hot plasmas [16]. The accuracy of the measured EUV lines around 360 Å is improved by the fact that calibration lines could be recorded with the same spectrometer settings.

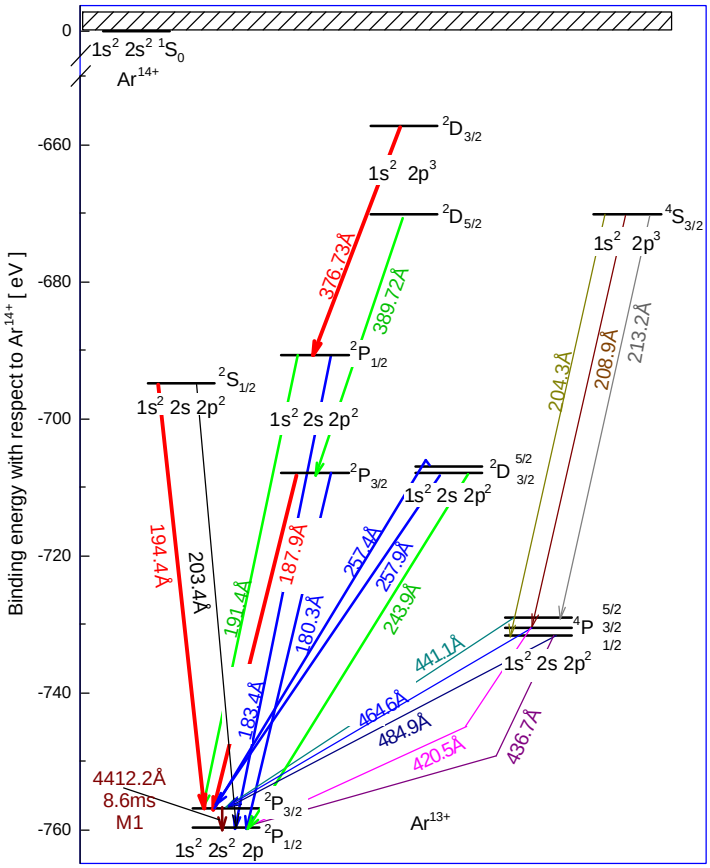

FIGURE 2. Energy level diagram for Ar^{13+} showing transitions observed in the EUV spectral range. The first excited level decays via an M1 transition to the ground state. The wavelengths are measured values.

For Be-like Ar^{14+}, the resonance line ($2s^2\ ^1S_0 - 2s2p\ ^1P_1$) at 221.16 Å and the intercombination line ($2s^2\ ^1S_0 - 2s2p\ ^3P_1$) at 424.02 Å are recorded, these being of special interest. In low density plasmas, e.g. active solar plasma regions, the $2s2p\ ^3P_1$ level can be depopulated significantly by electron collisions. The line ratio between the intercombination and the resonance line can therefore become sensitive to the electron density of the plasma [1]. At 1 keV EBIT beam energy and an electron density of $2\cdot10^{12}$ cm^{-3} a line ratio of 1.4±0.4 % was estimated. A further advantage of this line ratio is the fact that for spectrometers which allow detection of second order diffracted lines, both the resonance and the intercombination line can be observed with the same spectrometer settings at nearby wavelengths.

B-like Ar^{13+} has a particular structure of energy levels with an excited level in near proximity of the ground state (Figure 2). This $2s2p\ ^2P_{3/2}$ level decays with a radiative life time of about 9 ms via M1 emission at 4412 Å to the $^2P_{1/2}$ ground state and is used as diagnostic of the ion cloud distribution in EBIT and as a high precision test of QED [17]. All the EUV lines feeding the $^2P_{1/2}$ ground state and the closely-lying $^2P_{3/2}$ level have been recorded. The intercombination lines 441.1 and 420.5 Å from the transitions $2s^22p\ ^2P - 2s2p^2\ ^4P$ and the much stronger 376.7 and 389.7 Å lines originating from highly excited levels are considered to be valuable temperature diagnostic for plasmas.

In Table 2 we summarize the observed EUV lines for C-like Ar^{12+}. The weak forbidden transition $2s^2\ 2p^2\ ^3P_1 - 2s^2\ 2p^2\ ^1S_0$ at 659 Å and two intercombination lines for transitions $2s^2\ 2p^2\ ^3P_{1,\,2} - 2s\ 2p^3\ ^5S_2$ around 480 Å have been observed in agreement with predictions by Edlén [14] and the solar line list [15]. Several lines for transitions between highly excited levels have been measured in the wavelength range 160 to 250 Å and have previously been found in theta-pinch experiments [8]. Recently these lines have been calculated with the Flexible Atomic Code. This package calculates the atomic structure; atomic radiative and collisional processes based on relativistic configuration interaction with independent particle basis wavefunctions.

References

[1] U. Feldman, *Phys. Scr*. **63**, 276 (2001).
[2] K. Wilhelm et al., *Solar Phys.* **162**, 189 (1995).
[3] C. Biedermann, A. Förster, G. Fußmann, R. Radtke, *Phys. Scr.* **T73**, 360 (1997).
[4] R.L. Kelly, *Phys. Chem. Ref. Data* **Vol. 16** Suppl. 1 (1987).
[5] G.D. Sandlin, G.E. Brueckner, V.E. Scherrer, and R. Tousey, *Astrophys. J*. **205**, L47, (1976).
[6] K.P. Dere, *Astrophys. J.* **221**, 1062 (1978).
[7] K.G. Widing, *Astrophys. J.* **197**, L33 (1975).
[8] B.C. Fawcett, A.H. Gabriel and T.W. Paget, *J. Phys. B* **4**, 986 (1971).
[9] B. Edlén, *Phys. Scr*. **28**, 483 (1983).
[10] G. Liang, G. Dong, J. Zeng, *At. Data and Nucl. Data Tables* **88**, 83 (2004).
[11] C. Biedermann, R. Radtke, J.L. Schwob, P. Mandelbaum, R. Doron, T. Fuchs, G. Fußmann, *Phys. Scr*. **T92**, 85 (2001).
[12] W.A. Deutschman and L.L. House, *Astrophys. J.* **149**, 451 (1967).
[13] S.O. Kastner, A.K. Bhatia, and L. Cohen, *Phys. Scr.* **15**, 259 (1977).
[14] B. Edlén, *Phys. Scr*. **31**, 345 (1985).
[15] U. Feldman, W. Curdt, E. Landi, and K. Wilhelm, *Astrophys. J.* **544**, 508 (2000).
[16] C. Biedermann, R. Radtke, K.B. Fournier, Phys. Rev. **E66**, 066404 (2002).
[17] I. Draganic, J.R Crespo López-Urrutia, R. Dubois, S. Fritzsch, V.M. Shabaev, R. Soria Orts, II. Tupitsyn, Y. Zou, and J. Ullrich, Phys. Rev. Lett. **91**, 183001 (2003).